Vesicle-to-micelle transition in aqueous solutions of amphiphilic calixarene derivatives

Norberto Micali* and Valentina Villari
CNR-Istituto per i Processi Chimico-Fisici, Via La Farina 237, I-98123, Messina, Italy

Grazia M. L. Consoli, Francesca Cunsolo, and Corrada Geraci
CNR-Istituto di Chimica Biomolecolare, Via del Santuario 110, I-95028 Valverde, Catania, Italy
(Received 21 November 2005; revised manuscript received 27 January 2006; published 8 May 2006)

Structure and conformation of spontaneous self-assembled calix[8]arenes derivatives are studied by means of static and dynamic light scattering and electrophoretic mobility. These amphiphilic molecules are in the aggregated form in aqueous solution, in a wide range of *p*H; they take a vesicle structure in neutral and basic *p*H environment, but, in relatively strong acidic conditions (below *p*H=4.5), a transition from vesicle to micelle occurs. The structural change is driven by the surface charge density. At neutral *p*H calix[8]arenes take a negative surface charge, which prevents coagulation and ensures stability; at acidic *p*H the surface charge tend to become positive because of the protonation of the hydrophilic head. These *p*H-responsive aggregates, able to release an encapsulated hydrophilic guest, are promising systems for application as nanocarriers.

DOI: 10.1103/PhysRevE.73.051904 PACS number(s): 87.15.Nn, 82.70.Dd, 78.35.+c, 87.15.Tt

I. INTRODUCTION

Spontaneous self-assembly of molecular components in a well defined, discrete aggregated structure is common in natural systems (virus, collagen, muscular fibre, DNA, etc.). Drawing inspiration from the Nature, controlled self-assembly of specific amphiphilic molecules is of great interest in biophysics [1–4], biomimetic chemistry [5–7], and material science [8–10]. Appropriate functionalization of platforms is a valid strategy to produce amphiphilic structures able to self-assembly by a suitable balance between hydrophilic and hydrophobic components. Particularly interesting in this respect are calixarenes, which combine the properties of macrocyclic hosts and self-organizing systems. The lack of toxicity and the lack of immune response of calixarene derivatives [11,12] enable new applications of these macrocycles in biomedical and pharmaceutical sciences. Solid lipid nanoparticles, [13–16] stimuli-responsive vesicles and micelles [17–19] based on amphiphilic calixarenes have been reported.

The possibility of control of the self-assembly process of amphiphiles to obtain stable aggregates is fundamental for applications in drug delivery. Also important is the ability of aggregates themselves to respond to external stimuli as *p*H. It is known [20,21] that infected and tumor tissues have a lower *p*H than the physiological, so that *p*H-sensitive carriers destabilize and release the entrapped drugs.

Recently, some of us (Consoli *et al.* [22,23]) synthesized amphiphilic glyco- and glycosaminoacid-calix[n]arenes exposing terminal *N*-acetyl-glucosamine (GlcNAc) groups. Introduction of sugar moieties confers to the hydrophobic calixarene backbone good water solubility and specificity in molecular recognition [22,23].

In this paper, dilute aqueous solutions of GlcNAc-conjugated calix[8]arenes in which the sugar moiety is linked to the calixarene upper rim directly (Calix[8]GlcNAc) or via amino acid spacer (Calix[8]GlyGlcNAc) are studied by means of light scattering. It is shown that the amphiphilic nature of these calix[8]arene derivatives makes molecules organize in stable supramolecular structures and that this self-assembly is *p*H dependent. In acidic environment a transition from vesicles to micelles occurs, suggesting that these molecules are potentially useful as selective delivery systems of hydrophilic drugs.

II. EXPERIMENTAL SECTION

A. Material

The aqueous solutions of Calix[8]GlcNAc and Calix[8]GlyGlcNAc (see Fig. 1 for their molecular structure), whose synthesis procedure was described elsewhere [22,23], were investigated at a concentration of 62 μM, after one week from preparation. The time independence of the hydrodynamic radius (and of the scattered intensity) ensured that the thermodynamic equilibrium has been reached. The bidistilled water used to prepare solution at *p*H=7 has a conductance of 30 μS/cm.

Each solution at different *p*H values was prepared by dissolving a weighed amount of solute in the acidic or basic solution at the desired *p*H. A comparison with the static and dynamic properties of the solutions (form factor and diffusion coefficient of aggregates) prepared varying *p*H from 7 indicates that the same thermodynamic equilibrium is reached with both methods of sample preparation.

For the fluorescence measurements Calix[8]GlcNAc (62 μM) was dissolved in a rhodamine B aqueous solution at a concentration (3 mM) where self-quenching becomes important. Rhodamine is often used as low molecular weight drug model to demonstrate the existence of an aqueous compartment inside the aggregate [24] and the ability of supramolecular structures to act as carriers [25]. After a week the stabilized solution was purified from the free dye by

*Electronic address: micali@me.cnr.it

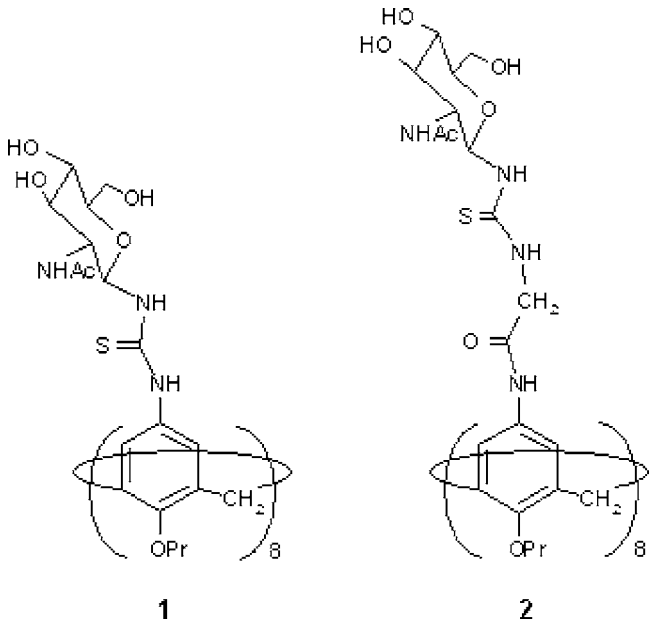

FIG. 1. Molecular structure of Calix[8]GlcNAc (1) and Calix[8]GlyGlcNAc (2). The symbols Pr and Ac indicate propyl (C_3H_7) and acetyl (CH_3CO) groups, respectively.

chromatographic gel filtration (Sephadex G-50) and fluorescence spectra collected.

B. Method

Light scattering experiments were performed by using a He-Ne laser source ($\lambda=633$ nm) at a power of 10 mW, linearly polarized orthogonal to the scattering plane, and a homemade computer controlled goniometric apparatus. The scattered light was collected in a pseudocross correlation mode through two cooled R943-02 photomultipliers at the same scattering angle.

In order to measure the depolarization ratio a Glan-Taylor polarizer was placed in the incident laser path and a Glan-Thomson analyser used for the scattered light. The value of the depolarization ratio, $I_{VH}(Q)/(I_{VV}(Q)-4/3I_{VH}(Q))\approx 0.003$ (I_{VV} and I_{VH} being the polarized and depolarized scattered intensity, respectively) indicates a very low depolarization. For the solutions containing smaller aggregates a Nd:yttrium-aluminum garnet laser ($\lambda=532$ nm) was used at a power of 100 mW.

Temperature was controlled within 0.01 °*C*. No changes were induced by increasing temperature from 20 °C to 40 °C and keeping the solutions some hours at the selected temperature. Therefore, in the paper all the results are reported at room temperature.

For the dynamic light scattering measurements the scattered light, collected in a self-beating mode, is analysed by a MALVERN 4700 correlator to build up the normalized intensity autocorrelation function [26,27]

$$g_2(Q,t)=\frac{\langle I(Q,0)I(Q,t)\rangle}{\langle I(Q)\rangle^2}, \tag{1}$$

where $|Q|=(4\pi n/\lambda_0)\sin(\theta/2)$ (θ being the scattering angle, n the refractive index of the solution, and λ_0 the wavelength of light in vacuum). For scattered electric fields obeying Gaussian statistics the Siegert's relation holds

$$g_2(Q,t)=1+a|g_1(Q,t)|^2, \tag{2}$$

where a is a constant depending on the experimental setup and $g_1(Q,t)=\langle E_s^*(Q,0)E_s(Q,t)\rangle/\langle I(Q)\rangle$ is the normalized scattered electric field autocorrelation function.

For diffusing monodisperse spherical scatterers with radius R, the normalized field autocorrelation function takes a simple exponential form, $g_1(Q,t)=\exp(-\Gamma t)$. Under the condition $QR\ll 1$, Γ is related to the collective diffusion coefficient, D, by the relation $\Gamma=DQ^2$. However, if the diffusing spherical scatterer is rigid, the latter relation is fulfilled as well. For polydisperse scatterers, the field autocorrelation function may be expressed as the Laplace transform of a continuous distribution $G(\Gamma)$ of decay rates: $g_1(Q,t)=\int G(\Gamma)\exp(-\Gamma t)d\Gamma$. The effective diffusion coefficient, $D_{eff}=\langle\Gamma\rangle/Q^2$ (where $\langle\Gamma\rangle=\int\Gamma G(\Gamma)d\Gamma$ is the mean decay rate), can be obtained from the standard cumulant analysis [26–28]:

$$\ln|g_1(Q,t)|=-\langle\Gamma\rangle t+1/2!\mu_2t^2-1/3!\mu_3t^3+\cdots, \tag{3}$$

with μ_n the moments of the distribution $G(\Gamma)$. The polydispersity index is related to the second moment μ_2 (variance) as $\mu_2/\langle\Gamma\rangle^2$ (for values lower than 0.3).

Due to the low concentration, the Einstein-Stokes relation, $R_H=k_BT/(6\pi\eta D_{eff})$, can be used to obtain the hydrodynamic radius R_H of the scatterers from their diffusion coefficient (k_B being the Boltzmann's constant, T the absolute temperature, and η the solvent viscosity).

For the static light scattering measurements the scattered intensity of the solvent is subtracted from that of the solutions; then the obtained angular profile is normalized by the scattered intensity of toluene used as reference. The normalized scattered intensity can be written as [26–28]:

$$I(Q)=NKM_wcP(Q)S(Q). \tag{4}$$

$P(Q)$ and $S(Q)$ being the normalized form factor and structure factor respectively, N the aggregation number, M_w the molecular weight of the molecule, c the mass concentration, and K the optical constant. For the scattering geometry of the experiment the latter quantity is

$$K=\frac{4\pi^2n^2}{\lambda_0^4N_A}\left(\frac{dn}{dc}\right)^2, \tag{5}$$

N_A being the Avogadro number.

It can be considered that, for the solutions investigated, the concentration is low enough that $S(Q)$ can be approximated to unity.

The electrophoretic mobility, μ, of the particles was measured by the Brookhaven ZetaPALS instrument, which is based on the principles of phase analysis light scattering. The light source is a laser diode at $\lambda=661$ nm (with a power of 30 mW), whose beam is split before impinging on the sample. A portion passes through the sample in a cell containing two electrodes which provide an oscillating electric field, $E(t)$; the other portion of the beam is used as reference, modulated at 250 Hz and then recombined with the scattered

beam. This geometry allows for measuring even small deviation of the frequency in the scattered light by performing a phase comparison between the detected signal and the imposed frequency.

If particles have zero mobility, the Doppler frequency of the recombined beam is equal to the modulation frequency and the relative phase is a constant. If a small mobility is present, $\mu = \mathbf{v}/\mathbf{E}$ ($\mathbf{v}$ being the velocity of the charged particles under the electric field $\mathbf{E}$), the phase change can be measured by a phase comparator. The amplitude-weighted phase difference, AWPD, can be written as [29]

$$\langle \phi(t) - \phi(0) \rangle = \langle A \rangle Q[\mu E(t) + V_c t], \tag{6}$$

where $\langle A \rangle$ is the amplitude of the Doppler signal, Q the exchanged wave vector, and V_c is a constant taking into account collective motions due to eventual temperature gradients. Typical value of the applied electric field amplitude used in the experiment is 8 V/cm. The value of mobility was extracted by using the ZetaPALS software by Brookhaven. Fluorescence measurements have been performed by using a JOBIN YVON HORIBA spectrofluorimeter model FluoroMax-3. The fluorescence spectra at pH=3 were corrected properly by measuring the fluorescence emission of rhodamine B solution at different pH values.

III. RESULTS AND DISCUSSION

The amphiphilic character of the molecules, due to the presence of both hydrophilic (glucosamine) and hydrophobic groups (aromatic plus propyl tail), drives the system to the formation of aggregates in aqueous solution.

In Fig. 2 the mean decay rate $\langle \Gamma \rangle$ of the correlation functions is shown as a function of the exchanged wavevector at different pH values; its Q^2 dependence indicates that aggregates undergo Brownian diffusion. Whereas Calix[8]GlcNAc aggregates dynamic (diffusion) does not seem to depend significantly on pH in the range from 4.5 to 12 (the effective diffusion coefficient changes from $D_{eff}=1.7\times10^{-8}$ cm^2/s to $D_{eff}=2\times10^{-8}$ cm^2/s), the diffusion of the Calix[8]GlyGlcNAc aggregates sensitively depends on it in the same pH range, varying from $D_{eff}=8.25\times10^{-9}$ cm^2/s to $D_{eff}=1.8\times10^{-8}$ cm^2/s. The corresponding mean hydrodynamic radii are reported in Fig. 3(a); for Calix[8]GlcNAc aggregates it is $R_H \approx 110$ nm and for Calix[8]GlyGlcNAc ones R_H progressively decreases from about 200 to about 100 nm. As expected for large thermodynamic aggregates, the polydispersity of the solutions is high [between 0.2 and 0.3, as obtained by the fitting of the correlation functions with Eq. (3) truncated at the second order]. This high polidispersity affects the Q^2 dependence of $\langle \Gamma \rangle$ causing the underestimated values of the mean rate decay at low Q, as it can be seen in Figs. 2(a) and 2(b).

At pH=3, for both samples, aggregates disappear to give rise to smaller objects having a hydrodynamic radius of about 5 nm. In Fig. 4 the mean decay rate of the correlation functions of both samples at pH=3 is shown. In Fig. 5 the comparison between the correlation functions at two different pH values is shown for Calix[8]GlcNAc solutions, as an example. The scattered intensity [see Fig. 3(b)] depends on

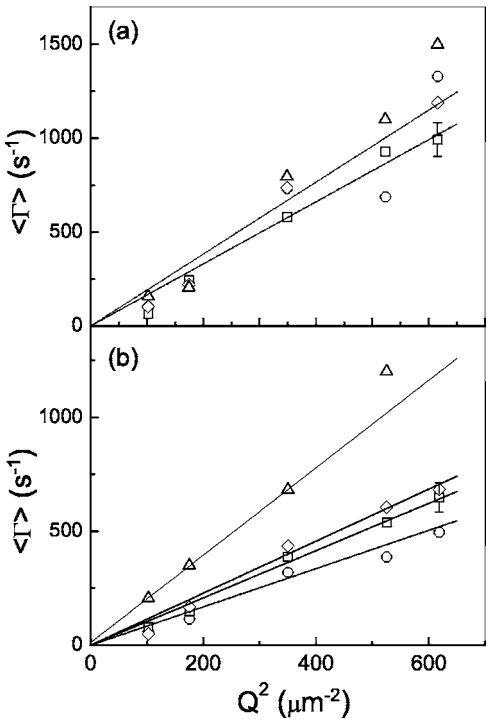

FIG. 2. Mean decay rate $\langle \Gamma \rangle$ of Calix[8]GlcNAc (plot a) and Calix[8]GlyGlcNAc (plot b) at pH=4.5 (circles), pH=7 (squares), pH=10 (diamonds), and pH=12 (up triangles). In plot (a) the fit of data at pH=7 and pH=10 are reported as examples.

pH accordingly with the hydrodynamic radius behaviour. At pH=3, because of the small size of the scatterers, it can be assumed that $P(Q) \approx 1$ [$S(Q) \approx 1$ because of the low concentration]. The measured intensity profile, in fact, shows no dependence on the exchanged wave vector. Thus, Eq. (4) (in which $\frac{dn}{dc}=0.18$ cm^3/g has been used) indicates that, at this pH value, micelles are present (with an aggregation number N of about 40 molecules), rather than isolated molecules.

At pH=12 the correlation functions seem to show the coexistence of small and large objects with a very large poly-

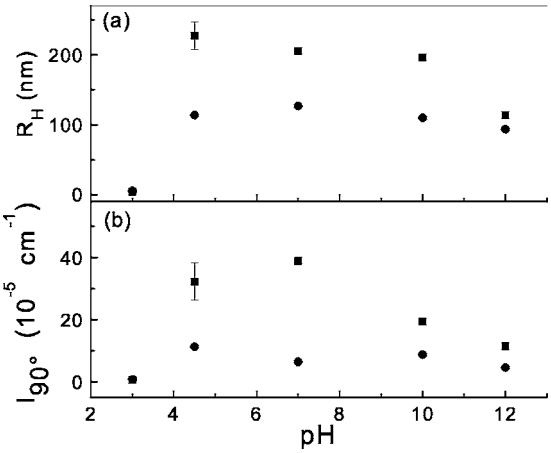

FIG. 3. Hydrodynamic radius (a) and absolute scattered intensity at 90° (b) as a function of pH for Calix[8]GlcNAc (circles) and Calix[8]GlyGlcNAc (squares).

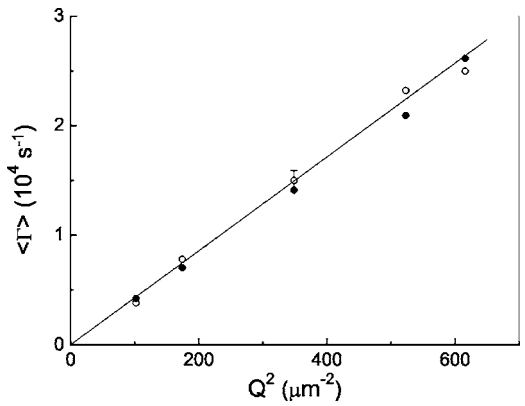

FIG. 4. Mean decay rate $\langle\Gamma\rangle$ of Calix[8]GlcNAc (hollow circles) and Calix[8]GlyGlcNAc (full circles) at pH=3 (D_{eff}=4.3 $\times 10^{-7}$ cm^2/s).

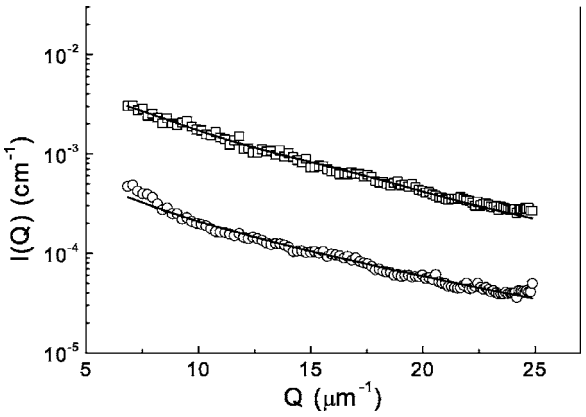

FIG. 6. Intensity profiles of Calix[8]GlcNAc (circles) and Calix[8]GlyGlcNAc (squares) at pH=7. The continuous lines are the fits according to the form factor described in Eq. (7).

dispersity. However, unlike the solutions at pH=3, large aggregates persist.

The decrease of the aggregate size on decreasing pH is in agreement with the results obtained recently by Lee and coworkers [17] on another calixarene in aqueous solution; they addressed it to the quarternization of the amine groups of the hydrophylic part of the molecule. This increases the surface area of the hydrophylic group causing the transition from vesicle to micelle. However, in the present investigation we find that also at pH=12 the equilibrium of the aggregate structure is affected.

In the pH range 4.5–12, the scatterer size is large enough to require a model for the form factor. The use of the homogeneous sphere model to describe the form of the aggregate does not agree with the experimental data. On the other hand, a vesicle conformation (also proposed in Ref. [17]), described by means of a thin shell model

$$P(Q) = \int \left[\frac{\sin(QR(x))}{QR(x)} \right]^2 f(x)dx, \tag{7}$$

leads to an intensity profile consistent with the experiment (the existence of an inner water compartment in the aggregate will be shown by the fluorescence results). The distribution function $f(x)$ (Gaussian) takes into account the static polydispersity of the solution. The vesicle thickness is too thin to be determined by light scattering because it does not contribute to the intensity profile in the Q range accessible to the technique.

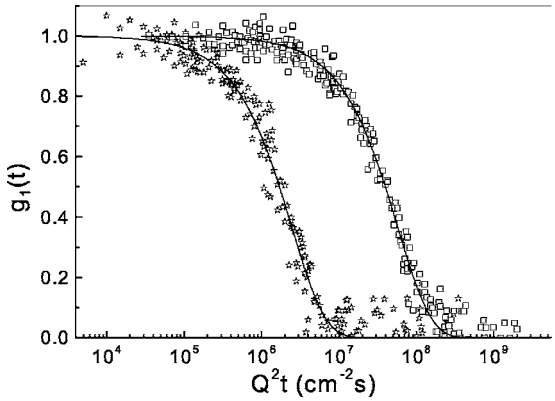

FIG. 5. Correlation functions of Calix[8]GlcNAc aqueous solution at pH=7 (squares) and at pH=3 (stars). The continuous lines are the results obtained by using the second order cumulant expansion Eq. (3).

In Fig. 6 the intensity profiles of Calix[8]GlcNAc and Calix[8]GlyGlcNAc are reported, at pH=7 as example, along with the fit obtained using Eqs. (7) and (4). From both profiles the average radius can be estimated as 150±50 nm and it does not seem to depend on pH sensitively in the range 4.5–12.

The gyration radius of vesicles cannot be determined directly, due to the unfulfilled Guinier limit; however, for vesicles (hollow spheres) it is equal to R.

In principle, the ratio ρ between gyration and hydrodynamic radius gives information on the internal structure of an aggregate; e.g., for vesicles ρ is expected to be equal to unity. In the case of these self-assembled calixarene molecules, this ratio is approximately 1 (within the experimental error). For polydisperse systems, however, the radius obtained by static and dynamic light scattering cannot be compared easily because different averages are evaluated [30,31]

$$R_h = \left[\sum_i f(R_{hi}) 1/R_{hi} \right]^{-1},$$

$$R_g = \left[\sum_i f(R_{gi}) R_{gi}^2 \right]^{1/2}.$$

It is worth noting that, although the monomers of these calix[8]arene derivatives have very similar molecular weight and the formed vesicles the same shape and very similar size, the absolute intensity of Calix[8]GlyGlcNAc is about ten times higher than that of Calix[8]GlcNAc. By the intensity value at Q=0 it emerges that vesicles formed by Calix[8]GlyGlcNAc have a higher aggregation number than Calix[8]GlcNAc, compatible with a bilamellar structure of Calix[8]GlyGlcNAc vesicles. The origin of these different structures could be ascribed to a different hydrophilic/hydrophobic balance due to the presence of the glycine

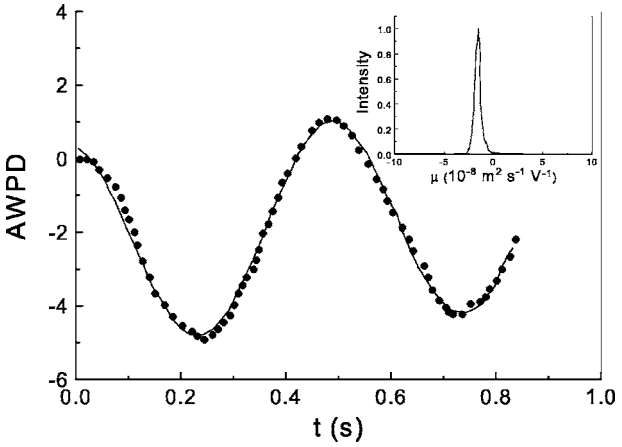

FIG. 7. Amplitude-weighted phase difference for Calix[8]GlcNAc solution at *p*H=7, as an example; the continuous line is the fit according to Eq. (6). The inset displays the result from conventional Laser Doppler electrophoresis.

group or to the hydrophilic chain length which favours a different geometrical packing.

Because the colloidal stability is ensured by the electric double layer, the measure of the aggregate mobility, and hence of the surface charge density, can allow for understanding the size modification as a function of *p*H. In Fig. 7 the typical amplitude-weighted phase difference measured for calixarene solution is shown together with the fit according to Eq. (6).

The obtained mobility is reported in Fig. 8; as it can be seen it is almost constant in the *p*H range from 7 to 12, whereas below *p*H=7 mobility becomes less negative to assume positive values at *p*H=3.

From the measured electrophoretic mobility one can estimate the ζ potential (i.e., the electrostatic potential at the shear plane where the liquid velocity is zero) of particles through the following relation (provided that $\zeta < 50$ mV) [32–34]:

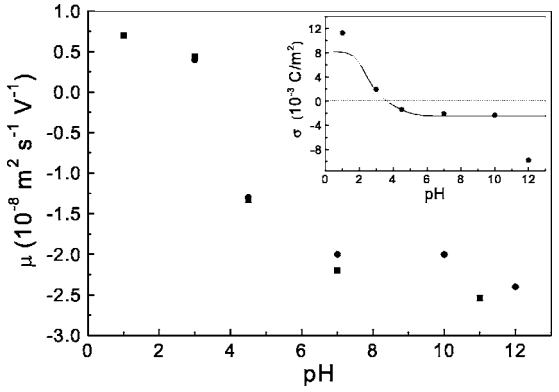

FIG. 8. Mobility of Calix[8]GlcNAc (circles) and Calix[8]GlyGlcNAc (squares) aggregates as a function of *p*H. The inset shows the surface charge density for Calix[8]GlcNAc aggregates, as obtained by relations (8) and (11); the continuous line is the theoretical curve according to the model described in the text, with $\log K_{H^+}=3.1$ and $S=0.23$ (see text for details).

$$\zeta = \frac{3}{2}\frac{\eta\mu}{\epsilon f(\kappa R)}, \tag{8}$$

where ϵ is the dielectric constant of the solvent, $\kappa^{-1} = \sqrt{\epsilon k_B T/(2e^2 I)}$ the Debye length, which characterizes the length scale of the double layer around the charged particle (e is the electron charge, I the ionic strength of the medium) and $f(\kappa R)$ is

$$f(\kappa R) = 1 + \frac{(\kappa R)^2}{16} - 5\frac{(\kappa R)^3}{48} - \frac{(\kappa R)^4}{96} + \frac{(\kappa R)^5}{96} + \left[\frac{(\kappa R)^4}{8} - \frac{(\kappa R)^6}{96}\right] e^{\kappa R}\int_{\kappa R}^{\infty}\frac{e^{-t}}{t}dt, \tag{9}$$

where R is the radius of the aggregate. In the limit of extended double layer ($\kappa R \gg 1$) it is $f(\kappa R)=1.5$ (Smoluchowski limit); in the opposite limit ($\kappa R \ll 1$) it is $f(\kappa R)=1$ (Hückel limit). For higher potential the relation between mobility and ζ potential requires numerical calculations [32,35].

The electrostatic potential, in the simple unidimensional case of a flat surface (Gouy-Chapman model), can be obtained by solving the Poisson-Boltzmann equation [36,37]

$$\frac{d^2\psi}{dx^2} = \frac{2n_0 Z}{\epsilon}\sinh\left(\frac{Z\psi}{k_B T}\right), \tag{10}$$

where ψ is the electrostatic potential, n_0 and Z are the number of ions per unit volume in the bulk solution far from the surface and their charge, respectively (for symmetric electrolytes). The surface charge density, σ, can be obtained provided that the potential at the shear plane is identified with the potential at the colloid surface, ψ_0. In fact, in the absence of specific ion absorption at the colloid surface (i.e., absence of ions in the region between the particle surface and the shear plane), Eq. (10) satisfies the condition [34]

$$\sigma = \frac{2\kappa\epsilon k_B T}{Z}\sinh\left(\frac{Z\psi_0}{2k_B T}\right). \tag{11}$$

The correction for the surface curvature of the colloid yields to [38,39]

$$\sigma = \frac{2\kappa\epsilon k_B T}{Z}\left[\sinh\left(\frac{Z\psi_0}{2k_B T}\right) + \frac{2}{\kappa R}\tanh\left(\frac{Z\psi_0}{4k_B T}\right)\right]. \tag{12}$$

In the inset of Fig. 8 the surface charge density is reported for Calix[8]GlcNAc as calculated from Eqs. (8) and (11) under the approximation that $\zeta \approx \psi_0$. The *p*H dependence of the vesicle surface charge density indicates that colloidal stability, found by light scattering results, corresponds to a negative surface charge (the ζ potential is about −35 mV). Such a negative charge can be addressed to the OH^- binding to the hydrophilic sugar head as observed in many nonionic amphiphiles [40,41]. On decreasing *p*H below 7, the surface charge density starts to increase to become positive at *p*H=3. This occurrence can be due to the progressive protonation of the Sulfur atom in the thioureido group (*–NHCSNH–*) [42]. The isoelectric point, where negative and positive charges balance, seems to occur at a *p*H value of

about 3.2. Below this value the vesicle to micelle transition is observed.

This *p*H dependence of the surface charge density can be taken into account by considering that each molecule in the aggregate possesses two sites: one occupied by the binding of OH^- ions and one which can be positively charged at low *p*H by the binding of the H^+ ions. The degree of binding of the negatively charged site is S (not dependent of *p*H in this model) and that of H^+ ions (with binding constant K_{H^+}) is [40]

$$f_{H^+} = \frac{10^{p\mathrm{H}} K_{H^+} \exp\left[-\frac{e\psi_0}{k_B T}\right]}{1 + 10^{p\mathrm{H}} K_{H^+} \exp\left[-\frac{e\psi_0}{k_B T}\right]}.$$

In this model the surface charge density of aggregates can be written as

$$\sigma = \frac{e}{a_s}[f_{H^+} - S], \tag{13}$$

with a_s the surface area per polar head, which is assumed to be the same for both H^+ and OH^- ions. [43]

In the inset of Fig. 8 the continuous line represents the theoretical *p*H dependence of the surface charge according to this model, using the values $\log(K_{H^+})=3.1$ and $S=0.23$. No significant differences are observed by using Eq. (12) instead of Eq. (11) for the calculation of σ.

The fact that both Calix[8]GlcNAc and Calix[8]GlyGlcNAc aggregates show the same electrophoretic mobility suggests that the binding constant of protons to the *NH* sites is too small (in the presence of the thioureido group) to modify the surface charge density of the colloid. The model described above agrees well with the experimental data in the *p*H range 3–10, but it is unable to describe the system in a strong acidic or basic environment. This occurrence could be due to the fact that the identification of the ζ potential with the surface potential, ψ_0, or the *p*H independence of a_s fail at extreme values of *p*H. However, it is likely that, at high *p*H value, a further absorption of OH^- ions makes the surface charge density more negative. By introducing another site for the OH^- binding (with binding constant K_{OH^-}) the agreement between theoretical and experimental data is improved at *p*H=12 (data not shown); however, finding the exact model for the surface charge density of vesicles is beyond the aim of this paper. The worth noting feature is that the vesicle-to-micelle transition is charge driven and occurs more efficiently when the surface charge density is positive. This result suggests that different factors (i.e., geometrical) there must exist along with the electrostatic repulsion. For example, the protonation of thioureido group in the inner part of the hydrophilic head tends to increase the surface area so increasing curvature. The *p*H sensitive behavior of these calix[8]arene derivatives appears to be useful for drug delivery. Their ability to encapsulate hydrophilic guests in the inner water pool and to release them in acidic environment has been tested by using fluorescence spectroscopy. In order to prove the existence of an aqueous compartment inside the vesicle, the dye rhodamine B has been used to mimic an encapsulated drug.

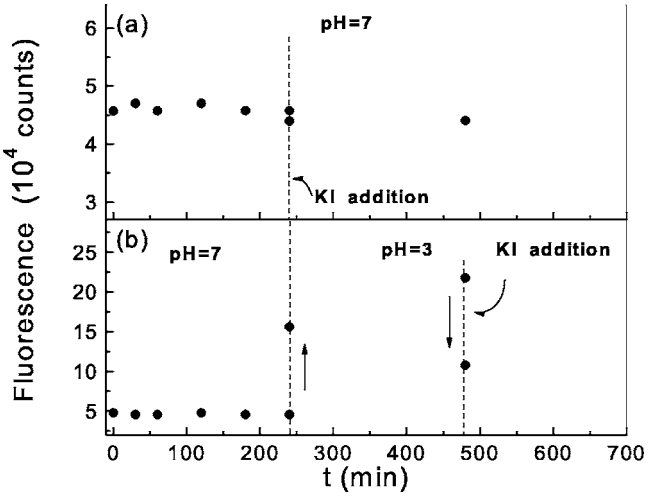

FIG. 9. Fluorescence emission at 575 nm (excitation wavelength 543 nm) as a function of time. (a) Fluorescence emission change after the addition of potassium iodide (1.6 M); the dashed line indicates the time at which the quencher is added to the solution. (b) Fluorescence emission change from *p*H=7 to *p*H=3 (dashed line at left) and after the addition of potassium iodide (1.6 M) (dashed line at right) at *p*H=3. Data are corrected properly by taking into account the fluorescence emission change of rhodamine B at *p*H=3.

The fluorescence emission of the purified (through chromatographic gel filtration) Calix[8]GlcNAc-rhodamine B aqueous solution is measured as a function of time; Fig. 9(a) shows that fluorescence emission at *p*H=7 remains constant, at least within 4 h. The addition of potassium iodide (a strong quencher) does not change the fluorescence emission significantly, so confirming that the dye is confined in the aqueous interior of vesicles and that vesicles do not undergo any leakage. The slight decrease of the fluorescence observed after the addition of the quencher can be due to the fluorescence quenching of those dye molecules present at the vesicle-water interface.

In order to understand if these calixarene vesicles are able to release the encapsulated dye in acidic environment, the *p*H of the Calix[8]GlcNAc-rhodamine B solution is lowered from 7 to 3. As it can be seen in Fig. 9(b), fluorescence emission abruptly increases because of the release of the dye in solution and the consequent dequenching. The following slow fluorescence increase on increasing time can be explained by the existence of a kinetics in the vesicle disruption.

The significant quenching after the addition of potassium iodide confirms that the dye has been released at *p*H=3 and is available in solution. These results are compatible with the vesicle-to-micelle transition observed in the light scattering experiments.

IV. CONCLUSION

The specificity [22,23] of calix[8]arene in molecular recognition made these molecules promising candidates in macromolecular biotechnologies. Therefore, characterization of

the self-assembly properties and conformation and size of aggregates in aqueous solution are fundamental for this purpose.

The results of the static and dynamic light scattering experiments indicate that molecules spontaneously self-assemble into stable vesicular aggregates. These aggregates maintain their size and structure in the *p*H range from 4.5 to 12, whereas at *p*H=3 a transition from vesicle to micelle is observed.

As shown by the measurement of the electrophoretic mobility, this structural change appears to be driven by the modification of the surface charge density because of the *p*H change. At neutral *p*H calix[8]arene takes a negative surface charge, like many nonionic amphiphiles in aqueous solution; this occurrence prevents coagulation and ensures stability. On decreasing *p*H below 4.5, the surface charge density starts to increase to become positive at *p*H=3.

A simple model is used to explain the experimental findings: each molecule in the aggregate possesses two sites, one occupied by the binding of OH^- ions (responsible for the negative surface charge density at *p*H=7) and one which can be positively charged at low *p*H by the protonation of the Sulfur atom of the thioureido group. Although this model is consistent with experimental data in the *p*H range 3–10, it fails in describing the system especially in a strong basic environment. This occurrence could be due to the fact that at high *p*H a further absorption of OH^- ions is responsible for the more negative surface charge density. The ability of these vesicle to encapsulate hydrophylic guests and to release them under acidic conditions has been proved by fluorescence spectroscopy measurements.

The reported investigation is devoted to the characterization of the self-assembly properties of calix[8]arene derivatives at different *p*H values and to prove their ability to behave as carriers of hydrophilic guests, rather than to exploit the caging effect of the calixarene molecule on hydrophobic molecules. The *p*H-sensitive behaviour of calix[8]arene aggregates, together with their ability of specific molecular recognition, open perspectives toward their application as selective delivery systems of hydrophilic drugs (e.g., in infections or tumors involving biological environment with high acidity).

[1] S. Kunsági-Máté, I. Bitter, A. Grün, G. Nagy, and L. Kollár, J. Biochem. Biophys. Methods **53**, 101 (2002).

[2] P. Shahgaldian, L. Quattrocchi, J. Gualbert, A. W. Coleman, and P. Goreloff, Eur. J. Pharm. Biopharm. **55**, 107 (2003).

[3] T. M. Weiss, T. Narayanan, C. Wolf, M. Gradzielski, P. Panine, S. Finet, and W. I. Helsby, Phys. Rev. Lett. **94**, 038303 (2005).

[4] S. U. Egelhaaf and P. Schurtenberger, Phys. Rev. Lett. **82**, 2804 (1999).

[5] R. Blumenthal, M. J. Clauge, S. R. Durell, and R. M. Epand, Chem. Rev. (Washington, D.C.) **103**, 53 (2003).

[6] T. M. Allen and P. R. Cullis, Science **303**, 1818 (2004).

[7] A. Mazzaglia, N. Angelini, R. Darcy, R. Donohue, D. Lombardo, N. Micali, M. T. Sciortino, V. Villari, and L. Monsú Scolaro, Chem.-Eur. J. **9**, 5762 (2003).

[8] A. Mueller and D. F. O'Brien, Chem. Rev. (Washington, D.C.) **102**, 727 (2002).

[9] D. E. Discher and A. Eisemberg, Science **297**, 967 (2002).

[10] H.-P. Hentze, C. C. Co, C. A. McKelvey, and E. W. Kaler, Top. Curr. Chem. **226**, 197 (2003).

[11] F. Perret, P. Shahgaldian, M. Mazzorana, and A. W. Coleman, *Book of Abstract, XIth International Symposium on Supramolecular Chemistry* (Fukuoka, Japan, 2000).

[12] M. H. B. G. Gansey, A. S. De Haan, A. S. Bos, W. Verboom, and D. N. Reinhoudt, Bioconjugate Chem. **10**, 613 (1999).

[13] P. Shahgaldian, M. Cesario, P. Goreloff, and A. W. Coleman, Chem. Commun. (Cambridge) 326 (2002).

[14] P. Shahgaldian, E. Da Silva, A. W. Coleman, B. Rather, and M. J. Zaworotko, Int. J. Pharm. **1**, 7348 (2002).

[15] P. Shahgaldian, J. Gaualbert, K. Aissa, and A. W. Coleman, Eur. J. Pharm. Biopharm. **55**, 181 (2003).

[16] A. Dubes, I. L. Moudrakovski, P. Shahgaldian, A. Coleman, C. I. Ratcliffe, and J. A. Ripmeester, J. Am. Chem. Soc. **126**, 6236 (2004).

[17] M. Lee, S.-J. Lee, and L.-H. Jiang, J. Am. Chem. Soc. **126**, 12724 (2004).

[18] M. Kellermann, W. Bauer, A. Hirsch, B. Schade, K. Ludwig, and C. Böttcher, Angew. Chem. **43**, 2959 (2004).

[19] E.-H. Ryu and Y. Zhao, Org. Lett. **6**, 3187 (2004).

[20] P. Vaupel, F. Kallinowski, and P. Okunieff, Cancer Res. **49**, 6449 (1989).

[21] L. Gerweck, Semin. Radiat. Oncol. **8**, 176 (1998).

[22] G. M. L. Consoli, F. Cunsolo, C. Geraci, T. Mecca, and P. Neri, Tetrahedron Lett. **44**, 7467 (2003).

[23] G. M. L. Consoli, F. Cunsolo, C. Geraci, and V. Sgarlata, Org. Lett. **6**, 4163 (2004).

[24] e.g., S. Pautot, B. J. Frisken, and D. A. Weitz, Langmuir **19**, 2870 (2003).

[25] e.g., G. Caponetti, S. J. Hrkach, B. Kriwet, M. Poh, N. Lotan, P. Colombo, and R. Langer, J. Pharm. Sci. **88**, 136 (1999).

[26] B. J. Berne and R. Pecora, *Dynamic Light Scattering* (Wiley-Interscience, New York, 1976).

[27] *Light Scattering: Principles and Development*, edited by W. Brown (Clarendon, Oxford, 1996).

[28] B. Chu, *Laser Light Scattering-Basic Principle and Practice*, 2nd edition (Academic, San Diego, 1991).

[29] J. F. Miller, K. Schätzel, and B. Vincent, J. Colloid Interface Sci. **143**, 532 (1991).

[30] J. Pencer and F. R. Hallett, Langmuir **19**, 7488 (2003).

[31] O. Stauch, R. Schubert, G. G. Savin, and W. Burchard, Biomacromolecules **3**, 565 (2002).

[32] A. V. Delgado, F. González-Caballero, R. J. Hunter, L. K. Koopal, and J. Lyklema, Pure Appl. Chem. **77**, 1753 (2005).

[33] F. McNeil-Watson, W. Tscharnuter, and J. Miller, Colloids Surf., A **140**, 53 (1998).

[34] R. J. Hunter, *Foundations of Colloid Science* (Oxford University Press, New York, 1986), Vols. I–II.

[35] R. W. O'Brien and L. R. White, J. Chem. Soc., Faraday Trans. 2 **74**, 1607 (1978).

[36] S. H. Behrens and M. Borkovec, Phys. Rev. E **60**, 7040 (1999).

[37] G. Gunnarsson, B. Jönsson, and H. Wennerström, J. Phys. Chem. **84**, 3114 (1980).
[38] A. L. Loeb, J. Th. G. Overbeek, and P. H. Wiersema, *The Electrical Double-Layer Around A Spherical Colloid Particle* (MIT Press, Boston, 1961).
[39] S. H. Behrens, D. I. Christl, R. Emmerzael, P. Schurtenberger, and M. Borkovec, Langmuir **16**, 2566 (2000).
[40] M. Johnsson, A. Wagenaar, and J. B. F. N. Engberts, J. Am. Chem. Soc. **125**, 757 (2003).
[41] S. Glasstone, *Textbook of Physical Chemistry* (Macmillan, New York, 1948), 2nd edition.
[42] J. Murgich, M. R. Santana, and J. A. Abanero, Magn. Reson. Chem. **25**, 115 (1987).
[43] The value of a_s used in the model is 1.5×10^{-17} m^2.